# NEAR-FIELD MEASUREMENT AND MODELING RESULTS FOR A FLIGHT-TYPE ARCJET: HYDROGEN ATOM

Mark W. Crofton and Teresa A. Moore
*Technology Operations, The Aerospace Corporation*
*M5/754, P.O. Box 92957, Los Angeles, California, 90009, U.S.A.*

Iain D. Boyd
*Department of Aerospace Engineering, University of Michigan*
*1320 Beal Avenue, Ann Arbor, Michigan, 48109-2140, U.S.A.*

Ideo Masuda
*DRTS Project Team, National Space Development Agency of Japan*
*2-1-1 Sengen, Tsukuba, Ibaraki, 305-8505, Japan*

Yoshifumi Gotoh
*Space Systems Department, Mitsubishi Electric Corporation*
*325, Kamimachiya Kamakura, Kanagawa 247, Japan*

## Abstract

Density, velocity, and temperature data were obtained in the near-field plume of an MR-509A arcjet thruster, using the nonintrusive, spatially resolved technique of two-photon laser-induced-fluorescence. The arcjet, a 1.8 kW model manufactured by PRIMEX Aerospace, will operate on the DRTS spacecraft under development by Mitsubishi Electric Corporation. The arcjet used for these experiments was modified by PRIMEX to operate on an $N_2/H_2$ gas mix simulating hydrazine decomposition products. Plume measurements were made on hydrogen atoms in the region from nozzle exit plane to the free molecular flow regime. The radial velocity distributions of H atoms were used to obtain their perpendicular translational temperatures. Comparisons of the H-atom signal intensity and radial linewidth with DSMC results were in good agreement except near the nozzle exit plane. The discrepancies are believed to be associated with quenching and self-absorption effects, although Stark broadening could be significant if the plasma density is higher than expected. The results improve the knowledge of near-field flow parameters for the MR-509 and ultimately improve the accuracy and understanding of predicted DRTS plume impingement torques and other plume phenomenology associated with the arcjet.

## Nomenclature

| | |
|---|---|
| a | Gaussian normalization parameter |
| b | Gaussian linewidth parameter |
| c | speed of light |
| e | elementary charge |
| $E_{kg}$ | transition energy between states k and g |
| f | oscillator strength |
| g | label for ground quantum state |
| g(ν) | Gaussian lineshape function |
| $\hbar$ | Planck's constant divided by $2\pi$ |
| $I_\nu$ | intensity of photon flux at frequency ν |
| k | label for intermediate quantum state |
| $k_\nu$ | absorption coefficient at frequency ν |
| l | label for final quantum state |
| L | absorption pathlength |
| m | electron mass |
| M | species molar mass |
| $N_i$ | density of species i |
| r | radial coordinate |
| T | temperature, K |
| z | axial coordinate |
| δ | two-photon absorptivity |
| $\varepsilon_0$ | permittivity constant |
| $\Delta\nu_D$ | Doppler Full-Width-Half-Maximum (FWHM) |
| $\hat{\varepsilon}_1$ | polarization vector for photon 1 |
| $\hat{\varepsilon}_2$ | polarization vector for photon 2 |
| $\vec{\mu}_{op}$ | electric dipole operator |
| ν | frequency |
| $\nu_0$ | center frequency |
| σ | absorption cross section |
| ω | angular frequency |

Subscripts

| | |
|---|---|
| D | Doppler |
| l | laser |
| Q | quenching |
| S | Stark effect |
| SA | self-absorption |

## Introduction

MR-509A/B hydrazine arcjet thrusters[1] will provide north-south stationkeeping for the Data Relay Test Satellites (DRTS) being developed for on-orbit operation commencing in 2001 and 2002. MELCO is the prime contractor to NASDA for DRTS. Despite the successful operation of PRIMEX Aerospace Corporation (PAC) arcjets on several U.S. satellites,[2] little quantitative information has been readily available concerning many of the thruster impacts on satellites of arbitrary configuration. To rectify this situation for the DRTS case with regard to attitude and orbit

Copyright © 1999 by the Japan Society for Aeronautical and Space Sciences. All rights reserved.

perturbations, and thermal loading associated with plume impingement, MELCO contracted with The Aerospace Corporation to perform experimental measurements coupled with theoretical analyses. This resulted in the first laser-induced fluorescence (LIF) and mass spectrometric studies for a flight-type arcjet thruster. A portion of the Aerospace experimental work concerned with the measurement of near-field parameters is described in this report.

Limited time was available for data gathering on the MR509A. This curtailed the data set that would otherwise have been obtained.

## Experimental Setup

Test Facility and Arcjet Operation

All experimental testing was performed at The Aerospace Corporation's Mechanics and Materials Technology Center. The test chamber is 5.5 m in length and 2.4 m in diameter. Test chamber vacuum was maintained by 16 VHS-400 diffusion pumps. During thruster operation at the nominal flow rate of 46.4 mg/s, test chamber pressure was maintained below $1\times10^{-3}$ Torr.

The thruster was mounted on a computer-controlled four-axis positioning system. The thruster axis could rotate in a horizontal plane more than 20 deg off the test chamber axis on one side and up to 10 deg on the other. This degree of freedom was not necessary during the LIF measurements; the arcjet nozzle was aligned with the test chamber long-axis and remained there. The vertical position of the arcjet was similarly fixed for the duration of the measurements. Two-axis positioning was performed in the axial and radial directions to explore the spatial dependence of near-field parameters.

Electrical power of 1.8 kW was supplied at 80 VDC to the power conditioning unit provided by PAC. Power was similarly supplied at 28 VDC to operate the protection and control electronics which had also been provided by PAC. These were not the flight-model units. The flight-model power processing unit for DRTS requires an input voltage of 33-51.5 VDC.[1]

A computer-controlled data acquisition and control system was supplied by Aerospace and set up to satisfy PAC specifications regarding arcjet operating limits. Arcjet operating voltage, current, inlet pressure, and flow rates were monitored at all times, and an automatic shutdown would have occurred had any process limit been exceeded during normal operations. Typical recorded parameters at the 46.4 mg/s nominal operating point at which all H and NH data were obtained are listed in Table 1. In practice, voltage and current levels varied somewhat but the power conditioner kept arcjet input power constant at 1.66 kW.

Table 1. Typical operating parameters during LIF measurements of H and NH in the MR-509 plume.

| Flow rate | Background Press. | Arc Voltage | Arc Current | Input Power | Thrust[a] | $I_{sp}$[a] |
|---|---|---|---|---|---|---|
| 46.4 mg/s | 0.8 mTorr | 109.7 V | 15.1 A | 1.66 kW | 235 mN | 517 s |

[a]Estimated from flight qualification data of Ref. 3, with 2% reduction for use of simulated $N_2H_4$ (2:1 mix of $H_2$,$N_2$)

Laser-Induced Fluorescence (LIF)

Laser-induced fluorescence is the preferred means of obtaining the near-field parameters discussed in this report. LIF offers high spatial resolution together with high sensitivity and results which are usually acceptable from a quantitative standpoint. Sub-millimeter spatial resolution is a requirement in the near-field, since the arcjet nozzle width at the exit plane is on the order of a centimeter. Sensitivity is a factor at the existing species densities, which range from $10^{12}$-$10^{16}$ $cm^{-3}$ in the probed region. The H atom ground state was probed via a two-photon LIF technique, as a one-photon approach can only probe excited states (unless the wavelength is in the xuv,[4] making photon generation and fluorescence detection difficult and limiting spatial resolution). Excited state properties, particularly density, may not replicate ground state distributions.

In the case of simultaneous absorption of two photons, the absorption cross section derived from perturbation theory is[5]

$$\sigma = \left[(2\pi)^2 / \hbar c^2\right] I\omega \left|M_{lg}\right|^2 g(\nu), \qquad (1)$$

where $M_{lg}$ is the two-quantum matrix element which may be written as

$$M_{lg}(\omega) = 2\sum_k \frac{< l|\hat{\varepsilon}_1 \cdot \vec{\mu}_{op}|k >< k|\hat{\varepsilon}_2 \cdot \vec{\mu}_{op}|g >}{E_{kg} - \hbar\omega}. \qquad (2)$$

For a strong two-photon transition the ratio $\sigma/I$ is $\approx10^{-30}$ $cm^4/W$. At low light intensities single photon absorption may be written in differential form as

$$-dI = \sigma I N_i dx, \qquad (3)$$

where dx makes an infinitesimal contribution to L. When multiple photon absorption is included, the cross section may be expressed as

$$\sigma_{tot} = \sigma + 2I\delta + \ldots, \qquad (4)$$

where $\delta$ is the two-photon absorptivity, and for two-photon absorption Equ. 3 becomes

$$-dI = 2\delta I^2 N_i dx. \qquad (5)$$

A typical two-photon cross-section $I\delta$ is about 7 orders of magnitude smaller than a one-photon cross-section. For molecules with a center of symmetry one-photon electric dipole transitions are allowed where two-photon transitions are forbidden, and vice-versa. This is not the case for the hydrogen atom, which is why it is possible to readily observe the $L_\beta$ transition in one- or two-photon absorption as well as one-photon emission.

Quenching of excited states may occur as a result of collisions with partners in other quantum states. This is usually a problem at high gas densities. For the arcjet, the sum of species densities at the nozzle exit plane is about $8 \times 10^{15}$ $cm^{-3}$. In LIF measurements, if the upper state lifetime is much shorter than the interval between quenching collisions, quenching effects can be neglected. This is the case for the n=3 $^2D_{3/2,5/2}$ levels of the hydrogen atom in most regions of the plume expansion, as the zero-pressure lifetime is about

16 ns. Quenching effects are to be expected inside the nozzle.

The LIF experimental setup assumed several different configurations, depending on the measurement of interest. A YAG-pumped dye laser operating at 10 Hz repetition rate was doubled in a KDP crystal, and generated ≥ 1 mJ per 6 ns pulse in the region 570-680 nm when operated on a suitable laser dye. The crystal was tuned via a tracking circuit to maintain maximum output despite temperature drifts and frequency tuning. The H atom two-photon excitation wavelength of 205 nm was generated by mixing the doubled dye laser output (307.5 nm) with the fundamental (615 nm), each of appropriate polarization, in a β-$BaBO_4$ crystal mounted on a manual angle-tuning translation stage. Pulse energy ≈0.5 mJ was obtained at 205 nm. Due to optical losses, only about half of this was present at the thruster plume. The LIF signal depended approximately on the square of the pulse energy at 205 nm.

After elevation to the appropriate height for entry into the vacuum chamber, the laser beam entered through a window and passed through the arcjet plume perpendicular to the arcjet thrust axis. A photo of arcjet and LIF optics in the test chamber is given in Fig. 1. To obtain an axial velocity measurement, an optic placed below the thruster steered the beam to a second optic sitting downstream and below the thrust axis. The latter optic steered the beam to intersect the plume at an angle of ≈ 40 deg with respect to the thrust axis, and in the correct location to be aligned with the fluorescence collection optics. The laser beam was focused with a fused silica lens of about 30 cm focal length because of the cross-section dependence on laser intensity (see Equ. 4). Fluorescence was collected by a 5-cm-diameter $MgF_2$ lens placed 18 cm away from the arcjet centerline. The slowly converging fluorescence beam was transmitted over a distance of 1.2 m to a reflector which steered it through a LiF window into the external environment. The fluorescence beam then passed through a 10 nm bandpass filter and entered a 0.125 m monochromator. Detection was accomplished by means of a Hamamatsu R955 photomultipler tube attached at the monochromator exit. A boxcar amplifier was used to integrate the signal. Alignment of the collection optics was accomplished using a HeNe laser propagated back from the monochromator entrance, or scattered light from the probe laser at the location of interest.

The laser pulse energy generating the H atom fluorescence was recorded together with the fluorescence signal using computerized data acquisition. Typically 30 shots were averaged per channel, and data points were obtained by averaging the fluorescence signal from each channel after normalizing according to the square of pulse energy.

Lineshapes were recorded by stepping the dye laser frequency, collecting signal for a suitable period, and repeating over the full range of the transition. Fundamental frequencies were obtained in vacuum wavenumbers using a pulsed wavemeter, typically accurate to about 0.01 $cm^{-1}$. The wavemeter was automatically calibrated at intervals with an internal helium-neon laser, but was subject to minor drifting behavior between calibrations which occasionally resulted in readout errors of up to 0.03 $cm^{-1}$. Lineshapes were typically fitted with a three parameter Gaussian function,

$$g(\nu) = a\exp\left(-\frac{1}{2}\left(\frac{\nu-\nu_0}{b}\right)^2\right) . \qquad (6)$$

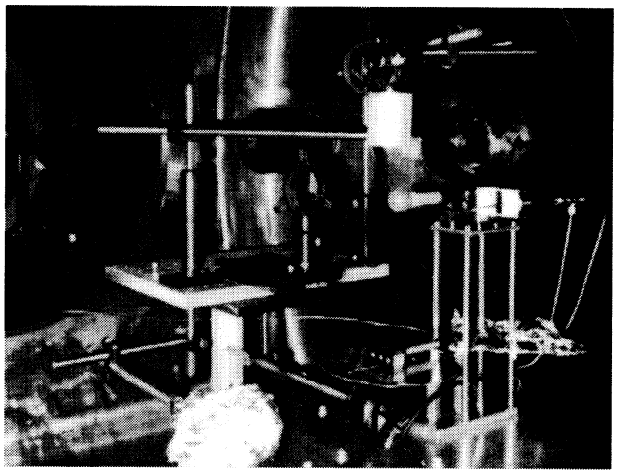

**Figure 1.** Photo of the experimental setup in the test chamber.

In many cases the transition center frequency was fixed, but the linewidth parameter and peak height were always variables. These parameters normally showed little dependence on whether the center frequency was fixed. The small residual baseline present in the experimental measurements was subtracted prior to fitting. The linewidth is determined largely by Doppler broadening and laser linewidth, although Stark- and self-broadening are issues near the arcjet exit plane. The Doppler width is determined by the Maxwell-Boltzmann distribution, and is related to temperature by

$$\Delta\nu_D = 2\sqrt{2\ln 2}\,b_D = 7.162\times10^{-7}\,\nu_0\sqrt{\frac{T}{M}} , \qquad (7)$$

where

$$b_D \cong \sqrt{b^2 - b_L^2 - b_S^2 - b_{SA}^2} . \qquad (8)$$

Since Stark broadening and self broadening do not give rise to a Gaussian lineshape, Equ. (8) is an approximation applicable where $b_S$ and $b_{SA}$ are effective widths and $b_{SA}^2, b_S^2 << (b_D^2 + b_L^2)$. The translational temperature (Kelvin) may be expressed as

$$T = 1.0811\times10^{13}\,\frac{M}{\nu_0^2}\,b_D^2 , \qquad (9)$$

where M is in amu and $\nu_0$ is in $cm^{-1}$. The laser FWHM linewidth (Full-Width-Half-Maximum) at the fundamental output of the dye laser (565-680 nm) was assumed to be 0.05 $cm^{-1}$ and Gaussian, in approximate agreement with the dye laser specifications and the linewidth suggested by a rough one-time analysis with the wavemeter.

Information about the n=3 upper states of the hydrogen atom is detailed in Table 2.[6] The allowed upper states of the two-photon absorption, which originates from the n=1 $^2S_{1/2}$ ground state, are n=3 $^2D_{3/2,5/2}$ and $^2S_{1/2}$. The transition intensity is about 7 times greater for the $^2D$ upper levels than for $^2S_{1/2}$. The fluorescence lifetime of $^2S_{1/2}$ is an order of magnitude greater. To obtain good signal to noise ratio on the $H_\alpha$ transition despite the intense continuous background from the arcjet plume, the fluorescence detection gate width

was set to about 13 ns. As a result, an insignificant amount of signal involving the n=3 $^2S_{1/2}$ level was collected.

For axial and radial measurements of LIF signal the laser frequency was positioned at the center of the transition lineshape. Some variation occurs in the lineshape as a function of radial and axial coordinate, therefore the observed raw signal is only an approximate indicator of H atom density. To obtain accurate density information it is necessary to know the lineshape as well as peak signal so that integrated signal strength can be obtained.

Table 2. Hydrogen atom fine and hyperfine structure (adapted from Ref. 6); the S state is taken as the origin. $\Gamma$ is the inverse lifetime, and $\omega$ gives energy with hyperfine splitting included while the second column neglects this splitting.

| State | Energy (MHz) | Hyperfine Energy (MHz) | $\omega$ ($10^9$ sec$^{-1}$) | $\Gamma$ ($10^9$ sec$^{-1}$) |
|---|---|---|---|---|
| 3 $^2S_{1/2}$ (F=0) | 0.0 | -39.457 | 0.0 | 0.0063 |
| 3 $^2P_{3/2}$ (F=1) | 2935.191 | -4.380 | 18.66274 | 0.1897 |
| 3 $^2P_{1/2}$ (F=1) | -314.898 | +4.382 | -1.70311 | 0.1897 |
| 3 $^2D_{5/2}$ (F=2) | 4013.197 | -1.577 | 25.45367 | 0.0647 |
| 3 $^2D_{3/2}$ (F=2) | 2929.859 | +1.577 | 18.66668 | 0.0647 |

## Numerical Approach

The flow inside the hydrazine arcjet is characterized by relatively low densities and very high temperatures. The Knudsen number (ratio of mean free path to boundary layer scale) of the nozzle flow varies from about 0.001 at the nozzle throat to about 0.1 at the nozzle exit plane. These values indicate that the flow will be in a state of thermochemical nonequilibrium. At the same time, on the flow axis near to the arc constriction, the ionization level can be as high as 40%.

These conditions place a heavy demand on attempts to perform accurate numerical simulations of the arcjet flow. At PRIMEX, a continuum-based computer code called KARNAC has been developed for computing arcjet flows. The code has performed very well in detail for hydrogen arcjet flows.[7] The accuracy of the code for hydrazine flows is less clear. There are several physical limitations of the KARNAC code. First, all energy modes are assumed to be in equilibrium. This precludes the possibility of freezing of the vibrational and rotational energy modes of the molecular species in the flow ($N_2$ and $H_2$). These are known to be loss mechanisms for arcjets. Second, by the time a Knudsen number of 0.1 is reached, the physical basis of the Navier-Stokes equations of fluid mechanics is no longer valid. Finally, because there is no thermal nonequilibrium included, important physical phenomena such as vibration-dissociation coupling are missing.

While we are primarily interested in analysis of the arcjet plume, for the reasons listed above, a more detailed analysis of the nozzle flow is also merited. In the present study, the direct simulation Monte Carlo method (DSMC)[8] is employed to compute both the nozzle and plume flows in a single simulation. The nozzle flow is begun just downstream of the constrictor in a region of the flow that is in the continuum regime. A startline for the DSMC computation is obtained from a solution generated by KARNAC and provided by Primex. The DSMC code includes the following physical phenomena:

(1) multi-species flow ($H_2$, H, $H^+$,$e^-$, $N_2$, N);

(2) rotational and vibrational relaxation;

(3) dissociation (with vibration coupling), ionization, and recombination reactions;

(4) ohmic heating.

The code is described in detail in Ref. 9 and has been extensively validated against experimental data for hydrogen arcjets.[10]

In terms of boundary conditions, the nozzle wall is treated as being diffuse with full accommodation of all energy modes to a fixed temperature of 1400 K. For the plume expansion, the experimentally determined back-pressure of 0.113 Pa is imposed. The analysis is performed for the nominal operating case of a flow rate of 46.4 mg/s and a power input to the arcjet of 1660 W.

The computation employs a grid of 500 by 70 cells in a structured grid. At steady state, a total of about 350,000 particles is employed. The computations provide mean particle quantities such as density, temperature, and velocity. Velocity distribution functions are also computed and this required the simulations to be performed over an extended period in order to reduce statistical scatter in the distributions collected.

## Results and Discussion

The fitted lineshapes obtained at several coordinates along the plume axis are plotted in Figs. 2 and 3. The Gaussian linewidths are plotted in Fig. 4.

The Doppler-free two-photon absorption spectrum of the n=3←n=1 transition[11,12] provides definitive relative intensities and peak positions. The spectrum shows that, while the relative intensities and peak positions do depend on electric field strength, the intense peaks remain within a 0.05 cm$^{-1}$ band. Since the frequency plotted in the lineshape (see Figs. 2,3) is the dye laser fundamental frequency, corresponding to the two-photon frequency sum divided by 6, the corresponding region in the plots spans less than 0.01 cm$^{-1}$. The energy separation of the most relevant levels for normal two-photon absorption, the D states, is only 1.1 GHz or 0.036 cm$^{-1}$, also insignificant compared to the observed linewidth. Fine structure splitting has therefore been ignored in the lineshape fitting.

All of the lineshapes in Figs. 2 and 3 are well-fit by a Gaussian function indicating that broadening mechanisms such as Stark effect and self-absorption, which add non-Gaussian character, are small compared to Doppler broadening. However, the experimental width of the transition very near the exit plane is noticeably broadened with respect to the DSMC prediction and with respect to a previous measurement on the NASA 1 kW arcjet.[13]

The degeneracy of same n, different *l* levels of the hydrogen atom, split only by spin and relativity effects, gives rise to a first-order Stark effect. However, lines with odd $\Delta$n, such as $H_\alpha$ and $H_\gamma$, $L_\alpha$ and $L_\gamma$, have a central Stark component that is unshifted in first order, whereas no such central component exists for even $\Delta$n transitions such as $H_\beta$ or $L_\beta$.[14]

As a result, the $\beta$ transitions exhibit a much larger static-field Stark effect and the broadening of $\alpha$,$\gamma$ transitions is dominated by ion collisions rather than electron collisions near the arcjet exit plane. The two-photon absorption is a $L_\beta$

transition, and therefore the theoretical tables should be reasonably accurate.

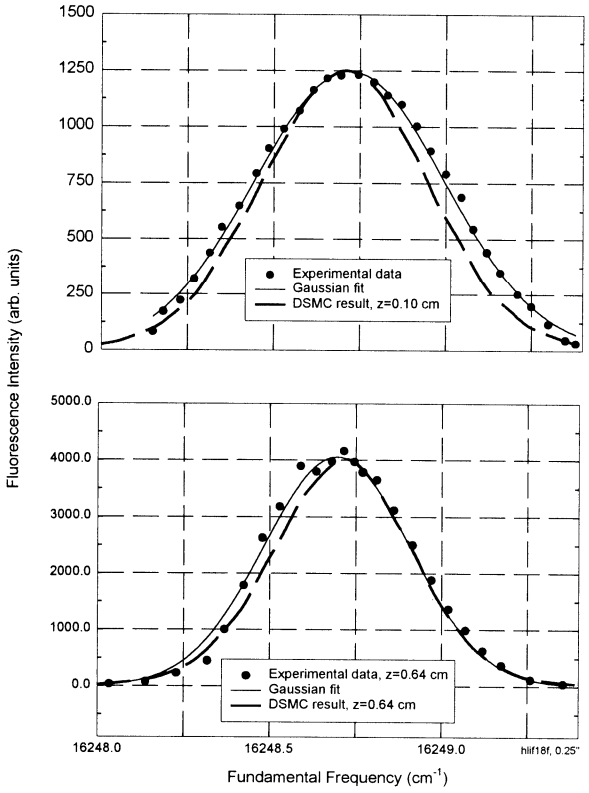


**Figure 2.** H atom lineshapes on plume centerline, at 1.0 (upper) and 6.4 (lower) ± 0.3 mm downstream from exit plane. The laser beam intersected the plume perpendicular to the thrust axis.

Stark broadening can be significant for the hydrogen atom even for electron density ≤ $10^{12}$ $cm^{-3}$, as it is the most sensitive atom to Stark effects. The analysis of previous data on the $H_\alpha$ lineshape near the exit plane of a $H_2$ arcjet concluded that Stark broadening is significant.[15] The effect of ion collisions with H atom dominates the Stark broadening under exit plane conditions, resulting in substantially greater broadening for some transitions at plasma density ≤$10^{15}$ $cm^{-3}$ than indicated in the standard theoretical compilations such as Vidal *et al.*[16]

The electron density was determined to be $8 \times 10^{13}$ $cm^{-3}$ at the exit plane of the hydrogen arcjet at 1.4 kW input power with linear power dependence, and to fall rapidly with axial distance in the downstream direction.[15] Although the electron density of an arcjet operating on $NH_3$ propellant may be considerably higher in the arc than in the pure hydrogen case,[17] there appears to be no experimental evidence available that a significant difference persists at the exit plane for hydrogen and simulated hydrazine arcjets. At $n_e = 1\times10^{14}$ $cm^{-3}$ the expected Stark lineshape of $L_\beta$ at 2500 K is double peaked, with a sharp minimum at line center and FWHM ~ 1.1 $cm^{-1}$ at the one-photon $L_\beta$ transition ($\Delta\nu/\nu_0 = 1.1\times10^{-5}$).

Not only does the lineshape broaden more than expected near the exit plane, the experimentally observed signal intensity drops precipitously (see Fig. 5) from its peak at z=0.8 cm. From a physical standpoint, the H atom density is expected to rise in the upstream direction as a monotonic

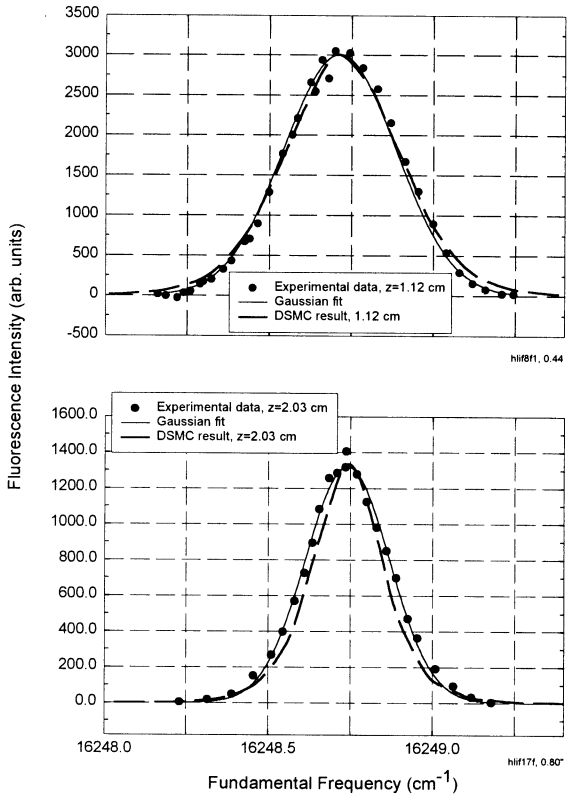


**Figure 3.** H atom lineshapes on plume centerline, at 11.2 (upper) and 20.3 (lower) ± 0.3 mm downstream from exit plane. The laser beam intersected the plume perpendicular to the thrust axis.

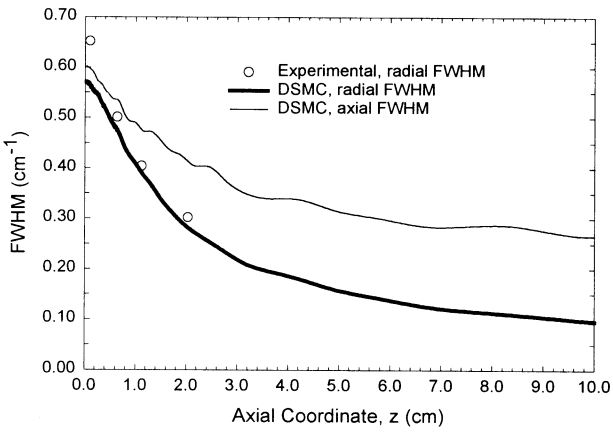


**Figure 4.** Experimental and theoretical FWHM on-centerline.

function. There are a number of reasons why the observed peak signal could decrease even as the density is increasing, including: (i) Stark and Doppler broadening, (ii) occlusion of fluorescence by the arcjet nozzle, (iii) inaccurate alignment of laser/arcjet/fluorescence detection apparatus, (iv) quenching effects, (v) self-absorption, and (vi) mixing of upper state wavefunctions by collisions and/or electric fields causing breakdown of selection rules and changes in fluorescence lifetime or fluorescence pathways.

The temperature does not change quickly enough for Doppler broadening to be a dominant factor, and Stark broadening does not appear to fit the observed lineshape – nor is the lineshape broadened sufficiently to explain the

observed intensity drop near the exit plane. At a distance of 1 mm from the exit plane fluorescence occlusion is negligible, and the alignment accuracy of the laser/arcjet/fluorescence detection apparatus is certainly better than 1 mm. This leaves (iv)-(vi) as potential explanations.

The decrease in fluorescence intensity due to the absorbing medium between probe volume and collection lens can be estimated from the relation

$$-dI_\nu(x) = k_\nu I_\nu dx \,, \tag{11}$$

where the 8-degree divergence (half-angle) has been neglected. Upon integrating through the medium, the result is

$$I_\nu(L) = I_\nu(0) e^{-\bar{k}_\nu L} \,, \tag{12}$$

where the further approximation has been made of replacing $k_\nu$ in the integral $\int_0^L k_\nu dx$ by an effective (average) value over the distance L. Using the relationship between transition oscillator strength and absorption coefficient,

$$\int k_\nu d\nu = \frac{e^2}{4\varepsilon_0 mc} N_i f \tag{13}$$

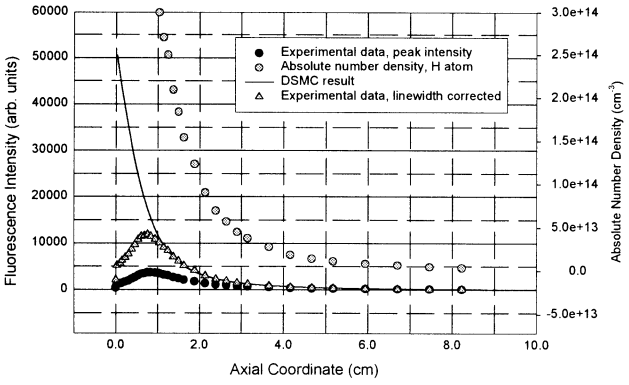


**Figure 5.** H atom axial profile.

the value of $\bar{k}_\nu L$ can be estimated. The value of $N_i$ is highly uncertain, and this quantity therefore determines the accuracy. Emission spectroscopy of medium power hydrogen arcjet plumes has measured II atom emission from many different levels and produced estimates of the number density.[18] At 6 kW the number density of n=3 at z=2.75 mm was about $6\times10^{10}$ cm$^{-3}$. Measurement of n=2 number density was much more difficult because of the vuv wavelength and the fact that the plume is optically thick with respect to the Lyman series. The background power level which pumps the $L_\alpha$ transition is estimated to be on the order of 1 mW cm$^{-2}$ near the exit plane[17] and may enhance n=2 with respect to other excited states. Under these conditions, the n=2 population density may be on the order of $10^{12}$ cm$^{-3}$. Starting from the Gaussian lineshape for T=2300K, about the value predicted by the DSMC calculation on-centerline for z=0.10 cm, the modified lineshape was computed by choosing $\bar{k}_\nu L$ such that the FWHM agreed with the experimental data. The result is shown in Fig. 6. The new lineshape obtained by including self-broadening can reproduce the experimental lineshape very well, better than least squares fitting to a Gaussian function. The value of $\bar{k}_\nu L$ needed was 0.45, corresponding to an average density of $1.6\times10^{12}$ cm$^{-3}$ over a pathlength of 5 mm.

The broadened lineshape near the exit plane is therefore believed to be caused by self-absorption rather than the Stark effect. An equivalent amount of Stark broadening requires several times higher plasma density than has been measured in the hydrogen arcjet, and would produce a sharp minimum at the center of the lineshape (self-absorption will produce a broad minimum at the line center when the absorption is strong). Self-absorption also can account for part of the reduction in peak signal intensity near the exit plane.

The mixing or redistribution of upper state level populations occurs in the presence of electric fields and during collisions. The electric field near the arcjet exit plane may be too low to cause mixing. Based on modeling and experimental results for n=3 H atoms populated through the n=3←n=1 2-photon absorption, just a few hundred mTorr of $H_2$ is sufficient to equilibrate the populations of the n=3 angular momentum states, L=0-2. The initial population

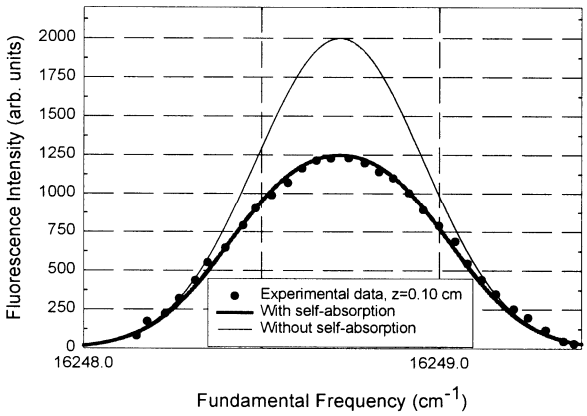


**Figure 6.** Self-absorption broadening near the exit plane.

distribution is about 12% s-state and 88% d-state as determined by the absorption cross-sections (selection rules prohibit initial population of the p-state). Upon equilibration, the populations become 11.1% s, 33.3% p, and 55.6% d, in accordance with the statistical weighting associated with level degeneracies. Due to the 159 ns lifetime of 3s and little change in its population, its contribution to the fluorescence signal can be neglected. In contrast, the population of 3p opens up two new fluorescence channels, 3P-2S and 3P-1S, with a branching ratio of 0.118. Even the 3P-2S channel contributes little to the fluorescence signal, due to its 46 ns lifetime.

The quenching rate constants for n=3 H atom are approximately $1.9\times10^{-9}$ and $2.8\times10^{-9}$ cm$^3$/s for $H_2$ and $N_2$, respectively.[19] With the assumed densities near r,z = 0 of $5\times10^{15}$ and $3\times10^{15}$ cm$^{-3}$ for $H_2$ and $N_2$, respectively, the partial pressures are estimated to be 0.39 and 0.23 Torr at the approximate plume temperature of 2300K. Assuming that quenching rates are proportional to pressure and independent of temperature or velocity,[20] use of the quantum yields from Table 2 of Ref. 18 indicates a combined quantum yield of 0.42 due to $H_2$ and $N_2$ quenching.

The combined signal reduction factor from quenching and self-absorption is therefore estimated to be

(0.42)(1250/2000)=0.26 at the z=0.10 cm location. After applying this factor and the correction of experimental data for linewidth, the comparison of data at z=1.25 cm and z=0.10 cm leads to the conclusion that the observed signal at z=0.10 cm is still low by a factor of 2. The reason for this is uncertain.

Using the relation

$$\Delta\nu \cong \sqrt{\Delta\nu_D^2 + \Delta\nu_I^2 + \Delta\nu_S^2 + \Delta\nu_{SA}^2} \qquad (14)$$

and Equs. 6-9, the temperatures listed in Table 3 were obtained. The lineshape analysis is approximate, as already discussed. No Stark or self-absorption corrections were made in the previous two-photon LIF study of H lineshapes in the NASA 1 kW hydrogen arcjet.[13]

The absolute H atom density was computed by extrapolating the mass spectrometer flux data at z=13 cm to a density figure[21] and applying $1/z^2$ scaling to connect with LIF data at 8.2 cm, enabling generation of the absolute density plot of Fig. 5. Using the ratio of densities at z=0.0 and 1.2 cm predicted by the DSMC results, a hydrogen atom density of $1.4\times10^{15}$ cm$^{-3}$ was computed at the exit plane, on centerline. A slight underestimate might be expected due to the extrapolation from 13 to 8.2 cm and the fact that the mass spectrometry detects only the atoms with virtually zero radial velocity. The density of $1.4\sim2.0\times10^{15}$ cm$^{-3}$ may then be compared with $5.0\times10^{15}$ cm$^{-3}$, the absolute density of the KARNAC result. The $H_2$ dissociation fraction is known to be 14.3%,[21] which is consistent with the $1.4\sim2.0\times10^{15}$ cm$^{-3}$ estimate.

The shift of peak signal when the laser source traversed the plume at centerline, 1.2 cm from the exit plane at 39 deg with respect to plume axis, was consistent with an H atom axial velocity of 9.2 ± 1.3 km/s. Due to alignment difficulties and time constraints, the peak velocity and axial velocity distributions were not pursued further.

Radial peak signal profiles are plotted in Fig. 7. Lorentzian fits gave significantly better results than Gaussian fits in most cases, but near the exit plane (z=0.10 cm) a combination of Lorentzian and Gaussian functions was needed. The function $\cos^4\theta$, where $\theta$ is the angle from thrust axis, did not give acceptable results. The more complex radial profile near the exit plane may be related to quenching effects. Quenching introduces a density-dependent factor $(1+\sum_i C_i N_i)^{-1}$, where $C_i$ is the product of radiative decay rate and quenching rate constant for the *ith* quenching species. This will modify the profile if $C_iN_i$ terms are large. The fluorescence lifetime was observed to be reduced at r,z = 0 in the hydrogen arcjet, relative to the natural lifetime, apparently due to quenching.[13] That quenching is still a minor effect at z=0.10 cm in the MR509A is apparent from the radial profile at that location, which does not show obvious flattening of the peak.

Due to the radial coordinate dependence of the width of the thermal velocity distribution, direct comparison of radial peak-signal profiles cannot be made to the DSMC results. The radial dependence of the thermal velocity FWHM was therefore calculated by the DSMC method, and Fig. 8 shows radial density profiles obtained from the product of calculated thermal width and peak signal, along with DSMC density profiles. The match between these profiles is very good.

The hydrogen atom is the most abundant species in the near-field of the arcjet plume, but is a minor momentum carrier because of its low atomic weight. Hydrogen atoms emerge from the arc excitation region with the highest velocity, both directed and random, because they have lower mass than other arcjet species. The directed and random velocity of H atoms is substantially reduced in the plume expansion by collisions with relatively massive partners. Separation of H from species like $N_2$ and NH is inevitable because of its relatively high perpendicular and parallel velocity components coupled with scattering away from the plume center by collisions with heavier species. The companion paper to the present study illustrates the species variability in near-field parameters.[22]

The agreement between experimental and DSMC results is generally very good for H atoms in the MR509A plume. The DSMC results were a valuable aid in the analysis of experimental data. As examples, DSMC results suggested that lineshapes were broadened by a non-Doppler mechanism near the exit plane, and provided a means to generate density profiles from peak-signal profiles.

The near-field plume data is valuable for the understanding of the arcjet flow and performance properties. The study of spacecraft plume impingement and torquing, as well as contamination and thermal loading, are best accomplished via DSMC calculations. Validation and improvements in code accuracy are accomplished by incorporating the results of plume measurements into the modeling analysis.[23]

## Acknowledgments

Thruster operations support was provided by D. Zube, J. English, and S. Crook of PRIMEX Aerospace, and J. Pollard, M. Worshum, L. Ortega, and E. Fournier of Aerospace Corporation. E. Beiting, J. Pollard, and R. Cohen provided valuable assistance in other aspects of the project. This manuscript is a revision of a 1998 report to MELCO, and its preparation was partially funded by the Aerospace IR&D program.

## References

1. Zube, D.M., Fye, D., Masuda, I., and Gotoh, Y., "Low Bus Voltage Hydrazine Arcjet System for Geostationary Satellites," AIAA Paper 98-3631, 34th Joint Propulsion Conf., Cleveland, July 1998.

2. Martinez-Sanchez, M., and Pollard, J.E., "Spacecraft Electric Propulsion," *J. Propulsion and Power*, Vol. 14, No. 5, 1998, pp. 688-699.

3. Smith, R.D., Roberts, C.R., Aadland, R.S., Lichtin, D.A., and Davies, K., "Flight Qualification of the 1.8 kW MR-509 Hydrazine Arcjet System," IEPC Paper 97-081, Aug. 1997.

4. Pollard, "Arcjet Diagnostics by XUV Absorption Spectroscopy," AIAA Paper 92-2966, 23rd Plasmadynamics and Lasers Conf., Nashville, July 1992.

5. Bischel, W.K., Kelley, P.J., and Rhodes, C.K., Phys. Rev. A13, 1829 (1976).

6. Van Baak, D.A., Clark, B.O., and Pipkin, F.M., "The 3 $^2S_{1/2}$ - 3 $^2D_{5/2}$ Interval in Atomic Hydrogen. I. Two-photon Line-shape Theory," *Phys. Rev. A* 19, 787 (1979).

7. Butler, G.W., Boyd, I.D., and Cappelli, M.A., "Nonequilibrium Flow Phenomena in Low Power Hydrogen Arcjets," Paper 95-2819, AIAA Joint Propulsion Conference, San Diego, CA, July 1995.

8. Bird, G.A., *Molecular Gas Dynamics and the Direct Simulation of Gas Flows*, Oxford University Press, 1994.

9. Boyd, I.D., "Monte Carlo Simulation of Nonequilibrium Flow in Low Power Hydrogen Arcjets," *Physics of Fluids*, Vol. 9, 1997, pp. 3086-3095.

10. Boyd, I.D., "Extensive Validation of a Monte Carlo Model for Hydrogen Arcjet Flow Fields," *Journal of Propulsion and Power*, Vol. 13, 1997, pp. 775-782.

11. Verkerk, P., Pinard, M., Biraben, F., and Grynberg, G., "1S-3S and 1S-3D Doppler-Free Two-Photon Transition in Hydrogen and Deuterium," *Optics Comm.* 72 (3,4), 202 (1989).
12. Booth, J.P., Derouard, J., Fadlallah, M., Cabaret, L., and Pinard, J., "Electric Field Measurements in Discharges by Doppler-free Two-photon Laser Stark Spectroscopy of Atomic Hydrogen," *Optics Comm.* 132, 363 (1996).
13. Wysong, I.J., Pobst, J.A., and Boyd, I.D., "Comparisons of Hydrogen Atom Measurements in an Arcjet Plume with DSMC Predictions," AIAA Paper 96-3185, July 1996.
14. Kelleher, D.E., Wiese, W.L., Helbig, V., Greene, R.L., and Oza, D.H., "Advances in Plasma Broadening of Atomic Hydrogen," *Physica Scripta* T47, 75-79 (1993)
15. Storm, P.V. and Cappelli, M.A., "Stark Broadening Corrections to Laser-induced Fluorescence Temperature Measurements in a Hydrogen Arcjet Plume," *Applied Optics* 35, 4913 (1996) .
16. Vidal, C.R., Cooper, J., and Smith, E.W., "Hydrogen Stark-Broadening Tables," *Astrophys. J. Suppl. Ser.* 25 (214), 37-136 (1973).
17. Crofton, M.W. "Spectral Irradiance of the 1 kW Arcjet Thruster from 80 to 500 nm" AIAA Paper 92-3237, July 1992.
18. Hoskins, W.A., Kull, A.E., and Butler, G.W., "Measurement of Population and Temperature Profiles in an Arcjet Plume," AIAA Paper 92-3240, 28th Joint Propulsion Conf., Nashville, July 1992.
19. Preppernau, B.L., Pearce, K., Tserepi, A., Wurzberg, E., and Miller, T.A., "Angular Momentum State Mixing and Quenching of n=3 Atomic Hydrogen Fluorescence," *Chemical Physics*, Vol. 196, 1995, pp. 371-381.
20. Terezawa, N., Ukai, M., Kouchi, N., Kameta, K., and Hatano, Y., "De-excitation of H(2p) in a Collision with a $H_2$ Molecule," *J. Chem. Phys.*, Vol. 99, No. 3, 1993, pp. 1637-1643.
21. Pollard, J.E., Masuda, I., and Gotoh, Y., "Plume Mass Spectrometry and Calorimetry with a Hydrazine Arcjet Thruster," IEPC Paper 99-041, 26th International Electric Propulsion Conf., Kitakyushu, Oct 1999.
22. Crofton, M.W., Moore, T.A., Boyd, I.D., Masuda, I., and Gotoh, Y., "Near-Field Measurement and Modeling Results for a Flight-Type Arcjet: NH Molecule," IEPC Paper 99-042, 26th International Electric Propulsion Conf., Kitakyushu, Oct 1999.
23. Nelson, D.A., Gotoh, Y., and Masuda, I., "A Simplified Model for the Prediction of Arcjet Plumes," IEPC Paper 99-043, 26th International Electric Propulsion Conf., Kitakyushu, Oct 1999.

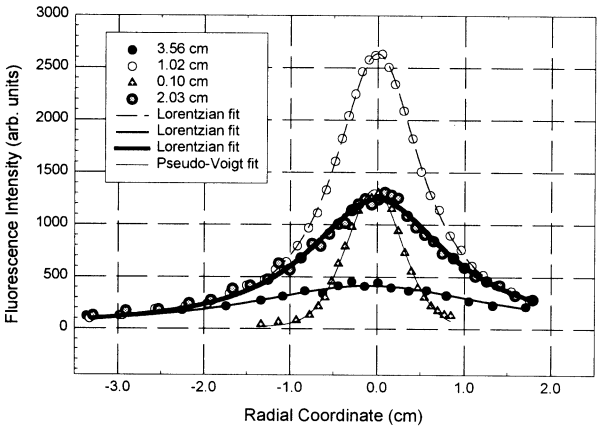


**Figure 7**. H atom radial profiles of peak intensity.

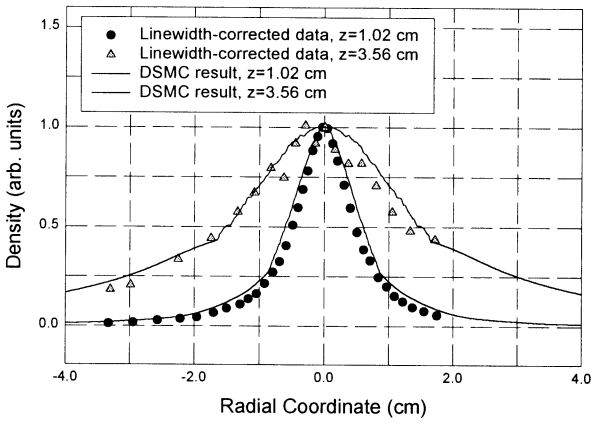


**Figure 8**. Radial density profiles.

Table 3. Hydrogen atom radial (perpendicular) translational temperatures

| (r,z) cm | FWHM @ 1025Å ($cm^{-1}$) | Temperature (K) | Error limits (K) |
|---|---|---|---|
| 0,0.10 | 3.91 | 2280 | ±300 |
| 0,0.64 | 2.99 | 1790 | ±150 |
| 0,1.12 | 2.42 | 1200 | ±100 |
| 0,2.03 | 1.81 | 670 | ±80 |